JACS
JOURNAL OF THE AMERICAN CHEMICAL SOCIETY

Article

pubs.acs.org/JACS

H-Bonded Donor–Acceptor Units Segregated in Coaxial Columnar Assemblies: Toward High Mobility Ambipolar Organic Semiconductors

Beatriz Feringán,[†] Pilar Romero,[†] José Luis Serrano,[‡] César L. Folcia,[§] Jesús Etxebarria,[§] Josu Ortega,[∥] Roberto Termine,[⊥] Attilio Golemme,[⊥] Raquel Giménez,*[,†] and Teresa Sierra*[,†]

[†]Departamento de Química Orgánica, Instituto de Ciencia de Materiales de Aragón (ICMA), Facultad de Ciencias, Universidad de Zaragoza-CSIC, 50009 Zaragoza, Spain

[‡]Departamento de Química Orgánica, Instituto de Nanociencia de Aragón (INA), Facultad de Ciencias, Universidad de Zaragoza, 50009 Zaragoza, Spain

[§]Departamento de Física de la Materia Condensada, Facultad de Ciencia y Tecnología, and [∥]Departamento de Física Aplicada II; Facultad de Ciencia y Tecnología, UPV/EHU, 48080 Bilbao, Spain

[⊥]LASCAMM CR-INSTM, CNR-NANOTEC Lab LiCryL, Dipartimento di Fisica, Università della Calabria, 87036 Rende, Italy

Supporting Information

ABSTRACT: A novel approach to ambipolar semiconductors based on hydrogen-bonded complexes between a star-shaped tris(triazolyl)triazine and triphenylene-containing benzoic acids is described. The formation of 1:3 supramolecular complexes was evidenced by different techniques. Mesogenic driving forces played a decisive role in the formation of the hydrogen-bonded complexes in the bulk. All of the complexes formed by nonmesogenic components gave rise to hexagonal columnar (Col_h) liquid crystal phases, which are stable at room temperature. In all cases, X-ray diffraction experiments supported by electron density distribution maps confirmed triphenylene/tris(triazolyl)triazine segregation into hexagonal sublattices and lattices, respectively, as well as remarkable intracolumnar order. These highly ordered nanostructures, obtained by the combined supramolecular H-bond/columnar liquid crystal approach, yielded donor/acceptor coaxial organization that is promising for the formation of ambipolar organic semiconductors with high mobilities, as indicated by charge transport measurements.

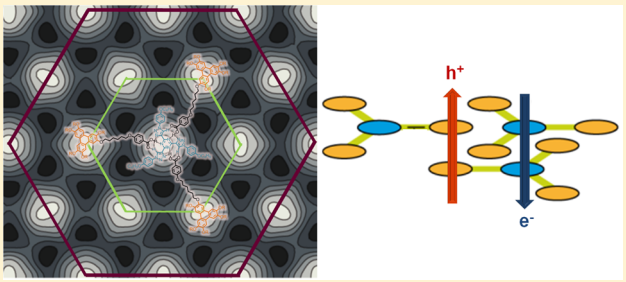

INTRODUCTION

The properties of functional materials are frequently enhanced when they have a well-organized internal structure, and, as a consequence, molecularly organized supramolecular materials are promising candidates for applications in organic (opto)-electronics.[1−4] In this respect, it is worth exploiting the ability of liquid crystals to self-organize in mesophases to obtain functional architectures.[5−8] In particular, discotic liquid crystals (DLC) are able to stack spontaneously into columns[9−11] to give one-dimensional structures of π-conjugated organic molecules. This organization facilitates long-range π-orbital overlap that allows, after appropriate charge injection, intracolumnar charge carrier mobilities with values close to or comparable to those of amorphous silicon. These features make columnar liquid crystals very attractive materials for use as organic semiconductors.[9−14]

It has been postulated that charge carrier transport in DLCs is intrinsically ambipolar;[15] that is, both hole and electron transport are possible,[16] but ambipolar behavior has only been found for a few DLCs.[15,17−22] The majority of DLCs contain electron-donor aromatic cores such as triphenylenes, phthalocyanines, and hexabenzocoronenes, and hole transport has been measured.[14] Triphenylene-based mesogens are among the most widely studied columnar liquid crystals,[23] and they show high hole mobility values in the columnar mesophase.[24−30] On the other hand, some electron-acceptor DLCs derived from azaheterocycles such as perylenebisimide, hexaazatriphenylene, and hexaazatrinaphthylene, to name a few, have been reported to show electron mobility.[31−36]

One approach to obtain ambipolar transport in a balanced way is to create a coaxial p/n heterojunction by using a donor/acceptor (D/A) system. Recent efforts rely on D/A covalent amphiphilic dyads[37,38] or supramolecular D/A dyads based on hydrogen bonding[39] or ionic interactions,[40] which form p/n heterojunctions in nanostructures by solvent-assisted methods to provide relevant photoconduction or ambipolar transport. The columnar mesophase approach has also been directed toward this end. In contrast to solvent-assisted methods, this approach

Received: July 1, 2016
Published: August 31, 2016

DOI: 10.1021/jacs.6b06792
J. Am. Chem. Soc. 2016, 138, 12511−12518

allows self-assembly in the bulk due to mesogenic forces that, with suitable molecular design, yield D/A segregation in the column. In this respect, the strategy is based on the covalent attachment of donor and acceptor units in dyads,[41−48] tryads,[49−51] or star-shaped[52−60] systems, with different degrees of order reported for the columnar mesophase. A few of them show ambipolar transport.[45,47,51,54] In addition to covalent systems, ambipolar transport has also been demonstrated for columnar mesophases formed by mixed donor and acceptor tapered-dendrons assembled by dipolar interactions.[61]

We recently described a new star-shaped molecule, tris(triazolyl)triazine, which can be readily prepared by means of click chemistry and has electron-acceptor character and gives rise to columnar liquid crystals.[62,63] Functionalization of this star-shaped core at the periphery can be achieved by covalent synthesis. In this way, the electron-acceptor tris(triazolyl)triazine was covalently linked through a flexible hexamethylene spacer to three peripheral electron-donor pentaalkoxytriphenylenes, and the resulting materials had columnar organization with a D/A coaxial segregation in which the columns were formed by a single type of discotic unit.[64] Moreover, the tris(triazolyl)triazine can be functionalized by a supramolecular approach. The presence of triazine and triazole rings means that the tris(triazolyl)triazine is able to establish hydrogen-bonding interactions with benzoic acids, thus leading to 1:3 complexes with hexagonal columnar mesomorphism.[65]

The results obtained in the previous study led us to envisage that the organization of donor and acceptors by supramolecular interactions, such as hydrogen bonding, in synergy with the mesogenic driving forces in columnar mesophases should be a favorable and versatile approach to achieve a high level of control over D/A segregation and hence ambipolar transport.

Accordingly, we report here a new combined supramolecular/columnar approach for the formation of star-shaped hydrogen-bonded complexes between a tris(triazolyl)triazine core and triphenylene-containing benzoic acids. This approach was developed with the aim of obtaining columnar liquid crystals with segregated columns of electron donors (triphenylene units) and electron acceptors (tris(triazolyl)triazine) in a more straightforward way than for covalently grafted compounds.[64]

The tris(triazolyl)triazine used as a core, $T3C_4$, has a *para*-butoxyphenyl substituent in each triazole ring. These butoxy terminal chains favor solubility in organic solvents, which is important for the formation of the supramolecular complexes by dissolution of a mixture of the components. Three different triphenylene-based benzoic acids (A-TPC_{10}, A-TPC_6, and A-TPC_4) were designed for the preparation of the supramolecular complexes. The three benzoic acids differ in the length of the terminal alkoxy chains of the triphenylene unit, that is, decyloxy chains (A-TPC_{10}), hexyloxy chains (A-TPC_6), and butyloxy chains (A-TPC_4), with the aim of studying the influence that these have on the organization in bulk. In all compounds, the triphenylene unit is linked to the benzoic acid by means of a hexamethylene spacer. Mixtures of the $T3C_4$ core and the aforementioned benzoic acids in a 1:3 ratio, respectively, were prepared to provide the target supramolecular complexes shown in Figure 1.

The formation of the supramolecular complexes was confirmed by spectroscopic techniques. All of the complexes show hexagonal columnar mesomorphism at room temperature with intracolumnar order and D/A segregation, as evidenced by X-ray diffraction and electron density maps. In addition, charge carrier mobilities were measured, and these highly ordered materials exhibit ambipolar charge transport properties.

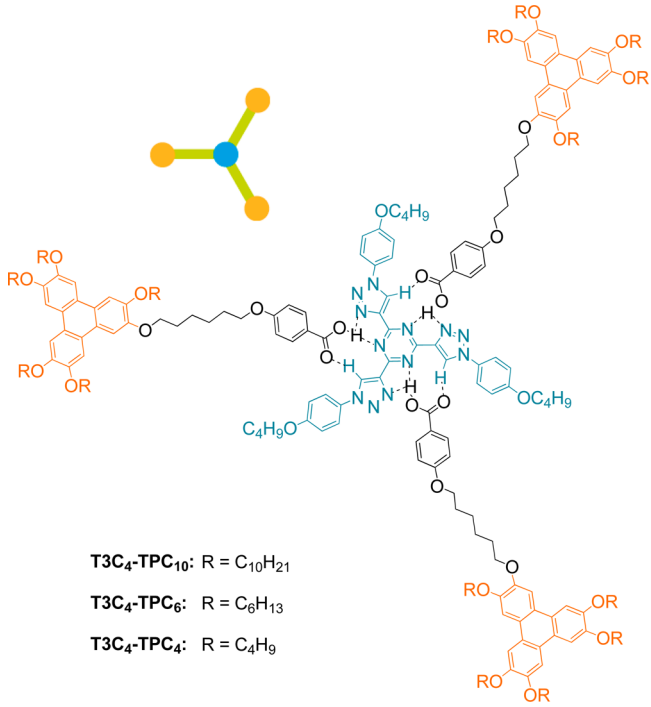

Figure 1. Molecular structure of the triphenylene-containing supramolecular complexes.

RESULTS AND DISCUSSION

Synthesis. The tris(triazolyl)triazine core ($T3C_4$) was synthesized by a previously reported procedure.[65] The triphenylene-based benzoic acids A-TPC_{10}, A-TPC_6, and A-TPC_4 were obtained according to the synthetic pathway outlined in Scheme 1. The synthetic procedures and characterization data are gathered in the Supporting Information. The required monohydroxypentaalkoxytriphenylenes (**1a−c**) were prepared in one step from *ortho*-dialkoxybenzenes by a previously described method.[64] The methyl benzoates **3a−c** were obtained by Williamson etherification of the monohydroxypentaalkoxytriphenylenes (**1a−c**) with methyl 4-(6-bromohexyloxy)benzoate (**2**), which in turn was prepared by Williamson etherification between methyl 4-hydroxybenzoate and 1,6-dibromohexane. The alkaline ester hydrolysis of **3a−c** with potassium hydroxide in 1,4-dioxane/water yielded the triphenylene-based benzoic acids A-TPC_{10}, A-TPC_6, and A-TPC_4.

The hydrogen-bonded complexes were prepared by dissolving a mixture of the tris(triazolyl)triazine core and the corresponding benzoic acid in a 1:3 ratio in dichloromethane. After evaporation of the solvent by continuous stirring at room temperature, the resulting mixtures were subjected to a thermal treatment in which the samples were heated to the isotropic liquid state and then cooled to room temperature.

Thermal Properties and Mesomorphic Behavior. The thermal properties of both the pure compounds and the H-bonded complexes were studied by polarizing optical microscopy (POM) and differential scanning calorimetry (DSC).

The pure compounds used for the preparation of the complexes are not liquid crystals. As described previously, $T3C_4$ does not have mesomorphic properties.[65] The triphenylene-based benzoic acids are not mesomorphic despite the fact

DOI: 10.1021/jacs.6b06792
J. Am. Chem. Soc. 2016, 138, 12511−12518

Scheme 1. Synthetic Procedure for the Preparation of the Triphenylene-Containing Benzoic Acids

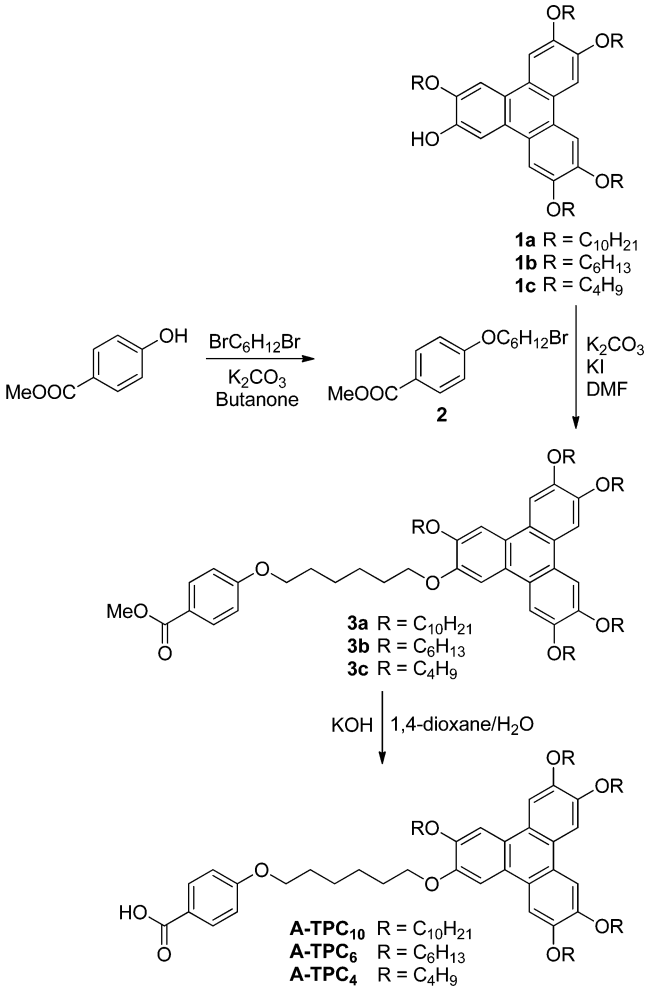

that they contain the triphenylene unit, which favors columnar mesomorphism. Instead, they are crystalline materials that, on cooling from the isotropic state, display different crystal forms (see Supporting Information).

All of the complexes appear as homogeneous materials by POM. Moreover, both complex T3C$_4$-TPC$_{10}$ and complex T3C$_4$-TPC$_6$ show liquid crystalline behavior, with textures characteristic of hexagonal columnar mesophases (Figure 2a and b). Furthermore, as deduced from the DSC cooling scans, both complexes retain the mesophase at room temperature (Table 1 and Figures S13 and S14), and crystallization was not observed.

Table 1. Thermal Properties of the Supramolecular Complexes and Structural Parameters Measured by X-ray Diffraction

complex	thermal properties (T, °C; [ΔH, kJ/mol])[a]	lattice parameters
T3C$_4$-TPC$_{10}$	I 80 [25.3] Col$_h$	a = 48.0 Å
	Col$_h$ 86 [27.9] I	c = 3.4 Å
T3C$_4$-TPC$_6$	I 129 [79.0] Col$_h$	a = 42.4 Å
	Col$_h$ 139 [89.7] I	c = 3.4 Å
T3C$_4$-TPC$_4$	I 17 g	
	g 29 I[b]	
	Col$_h$ 73 [24.0] I[c]	a = 39.6 Å[c]
		c = 3.4 Å[c]

[a]Thermal data are given from the first cooling process and the second heating process at a rate of 10 °C min^{-1}. [b]As-obtained complex. [c]After annealing above the glass transition for 90 h.

In contrast, the freshly prepared complex T3C$_4$-TPC$_4$ did not show any texture by POM, even on cooling below room temperature. Moreover, the DSC thermogram for the freshly prepared complex only shows a glass transition at 29 °C on heating, and this transition appears in immediately subsequent heating−cooling cycles (Figure S15). However, after the sample was annealed above this glass transition, a texture indicative of mesomorphic behavior was observed (Figure 2c). The columnar mesophase also developed slowly at room temperature. The heating cycle performed after annealing gave an endothermic peak at 73 °C (Table 1 and Figure S16), and this is consistent with POM observations.

It is noteworthy that, although none of the pure compounds are liquid crystals, mesomorphic properties are obtained from nonmesogenic components, a fact that provides strong evidence for the formation of the 1:3 complexes. Furthermore, the enthalpies obtained from the DSC thermograms are unusually high (Table 1), which suggests that the mesophases of these complexes are highly ordered.

X-ray diffraction (XRD) experiments allowed us to confirm that all complexes show hexagonal columnar mesomorphism at room temperature. XRD experiments were carried out on as-obtained samples for complexes T3C$_4$-TPC$_{10}$ and T3C$_4$-TPC$_6$, and after annealing above the glass transition in the case of complex T3C$_4$-TPC$_4$. Indeed, the X-ray pattern of T3C$_4$-TPC$_4$ immediately after the preparation of the complex (Figure S20) confirms that it is a disordered material. The diffractograms of the complexes at room temperature contain a large number of small-angle reflections indicating spacings with a ratio of d, $d/\sqrt{3}$, $d/\sqrt{4}$, $d/\sqrt{7}$, $d/\sqrt{9}$, $d/\sqrt{12}$, and $d/\sqrt{13}$. This is characteristic of a hexagonal lattice and corresponds to reflections (100), (110), (200), (210), (300), (220), and (310), respectively. At high

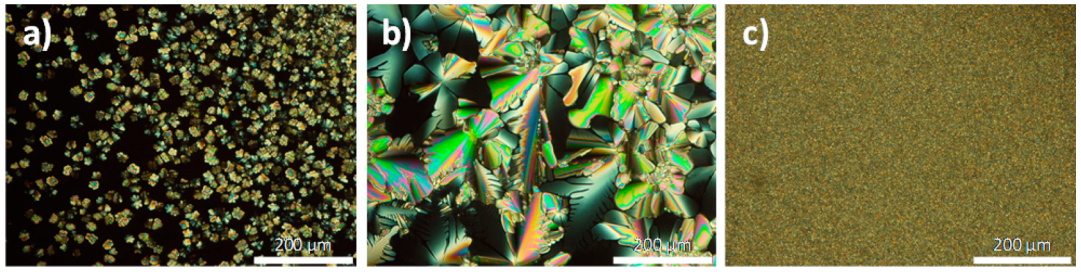

Figure 2. Microphotographs of the textures observed by POM for (a) T3C$_4$-TPC$_{10}$, Col$_h$, 85 °C (cooling), (b) T3C$_4$-TPC$_6$, Col$_h$, 117 °C (cooling), and (c) T3C$_4$-TPC$_4$, Col$_h$, room temperature (after annealing above the glass transition).

DOI: 10.1021/jacs.6b06792
J. Am. Chem. Soc. 2016, 138, 12511−12518

angles, all diffractograms show a diffuse halo at 4.5 Å, and this is characteristic of the liquid crystal state. In addition, an outer sharp reflection at 3.4 Å is observed, and this indicates a well-defined periodicity of the structure along the direction of the columnar axis. The diffraction data are summarized in Table S1, and the lattice parameters are listed in Table 1.

Interestingly, in all cases, the (100) reflection is weaker than the (200) reflection, which is the most intense (Figures 3 and S17−S19). The model proposed to account for this effect on the basis of a structure with hexagonal symmetry is shown in Figure 4. According to this model, tris(triazolyl)triazine (blue circles) and triphenylene (orange circles) units segregate into two different columns. This segregation takes place because the orientation of the links between blue and orange circles has two possibilities, (0°, 120°, 240°) or (60°, 180°, 300°) [see green and magenta schemes in Figure 5a]. Both orientations must occur with the same probability in the structure. However, the 2D positional order is easily explained if only one of the orientations takes place in a given 2D stratum. In this way, each layer is densely filled. On the other hand, both orientations can alternate randomly in successive strata as indicated in Figure 4a. Consequently, the projection of the structure along the columnar axis is that represented in Figure 4b, where blue and orange circles are centered on 6- and 2-fold symmetry axes, respectively. The figure shows the family of planes that correspond to the (100) point of the reciprocal lattice. They contain blue and orange circles and are separated by a distance d. However, as can be seen, planes that contain only orange circles are intercalated in the middle between the former, and this causes an interference effect that contributes to reduce the intensity of the (100) reflection [and also of the (h00) reflections for h odd]. In contrast, the (h00) reflections with even h values are reinforced as they receive the contribution of both kinds of planes (separated d/2). Furthermore, in the diffractogram of a partially aligned sample of T3C$_4$-TPC$_{10}$ (Figure 3a), which was oriented by mechanical treatment, the (001) reflection (due to the periodic stacking distance) is reinforced along the alignment direction, while the (100), (110), (200), and (210) reflections (low-angle reflections) are reinforced in the perpendicular direction. This pattern is consistent with a columnar mesophase in which columns are oriented along the rubbing direction.

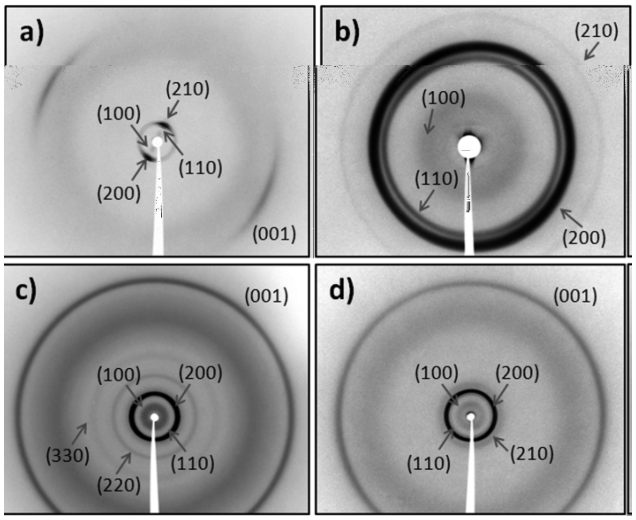

Figure 3. X-ray diffraction patterns recorded at room temperature of (a) a partially aligned sample of T3C$_4$-TPC$_{10}$, (b) T3C$_4$-TPC$_{10}$ (magnification of the low-angle region), (c) T3C$_4$-TPC$_6$, and (d) T3C$_4$-TPC$_4$ (after annealing above the glass transition).

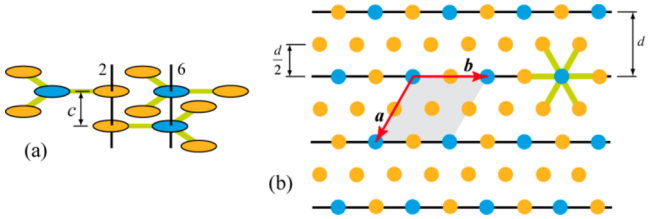

Figure 4. Scheme of the model proposed for the structure of the materials under study. Tris(triazolyl)triazine and triphenylene units are represented by blue and orange circles, respectively. (a) The orientation of the complexes alternates randomly in successive strata (separated by a distance c = 3.4 Å) in such a way that blue and orange columns segregate. (b) The projection of the structure on the (a, b) plane shows hexagonal symmetry. The family of (100) planes, separated a distance d, is indicated.

The number of molecules that contain the unit cell can be estimated from the experimental data in Table 1 and assuming a reasonable density value for these complexes close to 1 g cm^{-3}. The relationship between the density (ρ) of the complexes and the measured lattice parameters is given by the equation $\rho = (M \cdot Z)/(N_A \cdot V)$, where M is the molar mass of the 1:3 complex, Z is the number of molecules in the unit cell, N_A is Avogadro's number, and V is the unit cell volume ($V = a \cdot a\sqrt{3}/2 \cdot c \cdot 10^{-24}$). For all three complexes, a value of Z = 1 is obtained. These results indicate that there is one complex per unit cell, and this value is consistent with the formation of 1:3 complexes.

In an effort to seek further support for the proposed model, electron density distributions (Fourier maps) were calculated. These maps are constructed using the (hk0) reflections, and, therefore, they represent the projection of the structure on the (a, b) plane, as shown in the scheme in Figure 4b. The technical details of the procedure can be found in ref 66 (see also the Supporting Information).[66] The resulting maps (Figure 5) clearly indicate the segregation between columns of tris(triazolyl)triazine and columns of triphenylene, as indicated in Figure 4. It can be observed that triphenylene units (oval shape) are organized around the core T3C$_4$ (circular shape) with hexagonal symmetry.

Study of the Formation of the Complexes in the Mesophase. Additional support for the formation of 1:3 complexes in the mesophase was obtained by infrared spectroscopy and solid-state nuclear magnetic resonance (NMR) experiments.

The infrared spectra of both the complexes and the pure compounds were recorded at room temperature. For complexes T3C$_4$-TPC$_{10}$ (Figure S21) and T3C$_4$-TPC$_6$ (Figure 6a), the C═O stretching band is observed at around 1709 cm^{-1}, and this indicates complex formation between T3C$_4$ and benzoic acids.[65] This band appears at a different position from the C═O stretching band of the triphenylene-containing benzoic acids A-TPC$_n$. For these acids, the C═O stretching bands appear between 1683 and 1695 cm^{-1}, depending on the crystalline form, and correspond to the hydrogen-bonded dimers (see Supporting Information). Moreover, the band corresponding to the heterocyclic rings is shifted slightly to higher wavenumber (from 1566 to 1577 cm^{-1}) when the complex is formed.

As for XRD experiments, the infrared spectra of complex T3C$_4$-TPC$_4$ were recorded both immediately after preparation of

DOI: 10.1021/jacs.6b06792
J. Am. Chem. Soc. 2016, 138, 12511−12518

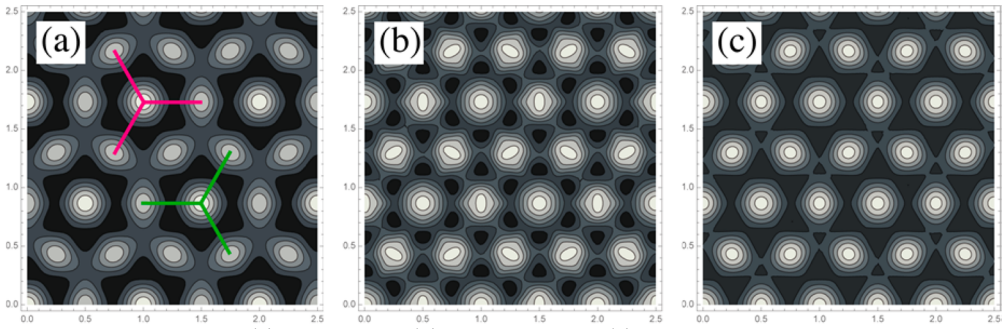

Figure 5. Electron density maps calculated for (a) $T3C_4$-TPC_{10}, (b) $T3C_4$-TPC_6, and (c) $T3C_4$-TPC_4 from the diffraction patterns at room temperature. The green and magenta schemes in (a) represent the two possible orientations of the complexes in different strata. For a given stratum only one orientation is present to give rise to a densely filled layer. The scales are in units of the cell parameter *a*.

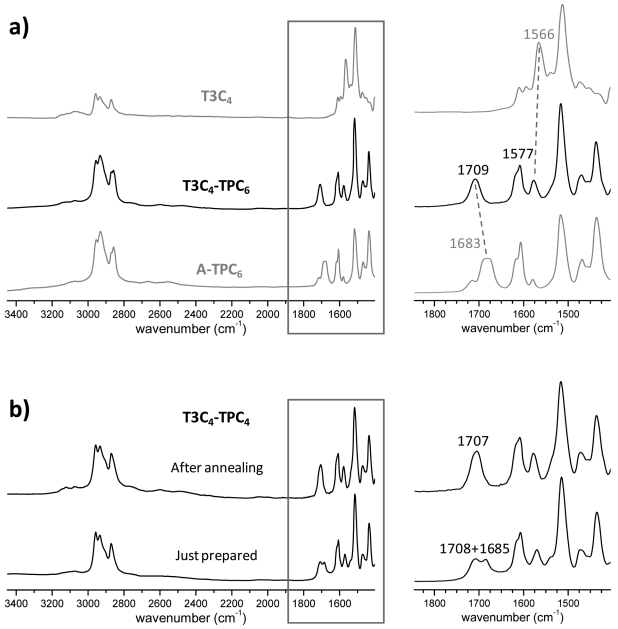

Figure 6. Infrared spectra recorded on KBr pellets at room temperature of (a) $T3C_4$, A-TPC_6, and complex $T3C_4$-TPC_6 and (b) $T3C_4$-TPC_4 as obtained (bottom) and after annealing above the glass transition (top). On the right, the 1850−1400 cm^{-1} region is shown.

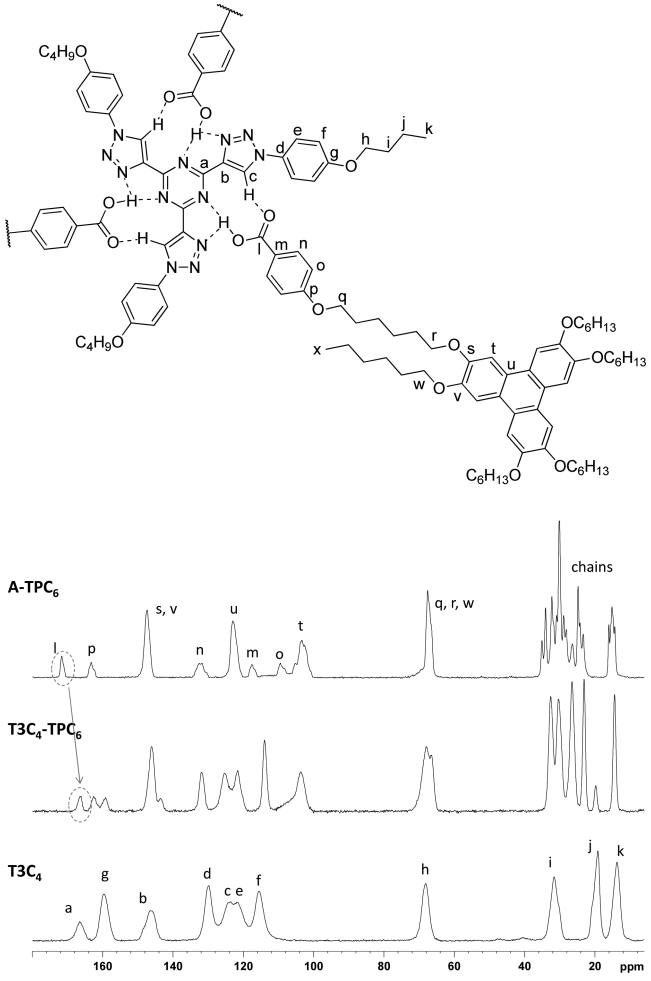

Figure 7. ^{13}C CPMAS NMR spectra of $T3C_4$, A-TPC_6, and the corresponding 1:3 complex, $T3C_4$-TPC_6, at room temperature. The most representative signals that shift upon complexation are indicated.

the complex and after annealing above the glass transition. The C═O stretching bands observed in the spectra are different (Figure 6b). The spectrum recorded just after the preparation of the complex shows two C═O stretching bands at 1708 and 1685 cm^{-1}, which correspond to the complex and the dimer of the benzoic acid A-TPC_4, respectively. The presence of these two C═O stretching bands suggests that the complex is only partially formed. However, after annealing, a single C═O stretching band is observed at 1707 cm^{-1}, which is similar to that in the other complexes and confirms the formation of the 1:3 complex $T3C_4$-TPC_4.

The ^{13}C cross-polarization magic-angle spinning (^{13}C CPMAS) NMR spectra of the core $T3C_4$, the acid A-TPC_6, and the corresponding complex, $T3C_4$-TPC_6, were recorded at room temperature (Figure 7). According to previous results,[65] the most significant evidence for the formation of the complex in a 1:3 stoichiometry is the shift of the signal corresponding to the carbon atom of the carbonyl group. In the spectrum of the acid A-TPC_6, a signal at 171.6 ppm, which corresponds to the dimeric form of the acid, is observed. In the spectrum of $T3C_4$-TPC_6, this signal is not observed, but a signal appears at 166.2 ppm, which is assigned to the carbonylic carbon and indicates that all of the acid forms the complex in a 1:3 stoichiometry. The signal corresponding to the carbon atom of the triazine ring must be also shifted to lower ppm,[65] together with other signals, but it is difficult to assign these shifts due to signal overlap.

Electrochemical and Charge Transport Properties. Cyclic voltammetry experiments were performed to study the electrochemical properties of the complexes (Figures S25−S27).

DOI: 10.1021/jacs.6b06792
J. Am. Chem. Soc. 2016, 138, 12511−12518

Table 2. Electrochemical Data for Complexes $T3C_4$-TPC_{10}, $T3C_4$-TPC_6, and $T3C_4$-TPC_4

complex	E^{red} vs Ag/AgCl (V)	E^{red} vs FOC (V)[a]	E^{ox} vs Ag/AgCl (V)	E^{ox} vs FOC (V)[a]	HOMO (eV)[b]	LUMO (eV)[c]
$T3C_4$-TPC_{10}	−1.70	−2.13	1.05	0.62	−5.42	−2.67
$T3C_4$-TPC_6	−1.60	−2.03	1.07	0.64	−5.44	−2.77
$T3C_4$-TPC_4	−1.58	−2.01	1.05	0.62	−5.42	−2.79

[a] $E_{1/2}$ = 0.43 V vs Ag/AgCl. [b] $E_{HOMO} = -e[E^{ox}$ vs FOC + 4.8 V]. [c] $E_{LUMO} = -e[E^{red}$ vs FOC + 4.8 V].

Table 3. Charge Mobility Values for Complexes $T3C_4$-TPC_{10}, $T3C_4$-TPC_6, and $T3C_4$-TPC_4

	mobility[a] ($cm^2\ s^{-1}\ V^{-1}$)		
	$T3C_4$-TPC_{10}	$T3C_4$-TPC_6	$T3C_4$-TPC_4
hole	$(8 \pm 6) \times 10^{-4}$	$(9 \pm 4) \times 10^{-3}$	$(1 \pm 0.3) \times 10^{-2}$
	$[(1.2 \pm 0.1) \times 10^{-8}]$	$[(4 \pm 1) \times 10^{-9}]$	$[(8 \pm 1) \times 10^{-9}]$
electron		$(7 \pm 5) \times 10^{-2}$	$(6 \pm 3) \times 10^{-3}$
	$[(2 \pm 0.6) \times 10^{-8}]$	$[(2 \pm 0.8) \times 10^{-6}]$	$[(9 \pm 2) \times 10^{-7}]$

[a] In the upper row, the average mobility in the higher range is shown. The value in square brackets is the average mobility in the lower range.

The cyclic voltammograms were recorded on drop-cast films of the complexes from solution in CH_2Cl_2, and the measurements were performed in an acetonitrile solution of tetrabutylammoniumhexafluorophosphate (0.1 M). One reduction wave, corresponding to the tris(triazolyl)triazine core, and oxidation waves corresponding to the triphenylene units were observed, and these are consistent with the electron acceptor or electron donor character of these units, respectively (Table 2). The HOMO and LUMO energy values, calculated from the oxidation and reduction waves, are approximately −5.4 and −2.7 eV, respectively, for all three complexes (Table 2).

The charge transport properties were measured by the space charge limited current (SCLC) method, as described in the Supporting Information. With this technique, mobility can be extracted from current/voltage characteristic curves if enough charges are injected form the electrodes and the SCLC regime is reached. Because charges have to travel between two electrodes, in anisotropic materials the measured mobility reflects the macroscopic degree of order and the orientation of the phase symmetry axes with respect to the electrodes. It is possible to measure charge mobility following several other experimental methods. Among the most common ones is the so-called time of flight (TOF) technique, where a short light pulse is used to generate charges close to the surface of a sample: the resulting transient current generated by an applied electric field is measured, and mobility is obtained if the thickness of the sample is known. In anisotropic materials, TOF mobility depends strongly on the size and on the orientation of different orientational domains, exactly as in the case of SCLC. Orientational issues are also important when considering mobility measurements extracted from field effect transistors (FET). In this case, what is measured is the current flowing, between the source and drain electrodes, through the first few molecular layers over the insulator: the measured value of mobility is determined by the orientational order at the sample/insulator interface, which can be controlled only to some extent by using specific surface treatments. Mobility can also be obtained from measurements of time-resolved microwave conductivity (TRMC), often following charge generation from an electron pulse. In this case, given the very short diffusion distance covered by charges during the measurement time, the measured mobility is not sensitive to orientational order. However, the main drawback of such an approach is that hole and electron mobilities cannot be distinguished, and this is a major problem in ambipolar materials.

One of the requirements of SCLC method is to have an ohmic contact between the injecting electrodes and the HOMO or LUMO levels to measure hole mobility and electron mobility, respectively. For hole mobility measurements, the cells were prepared with a glass covered by indium tin oxide (ITO) and another one covered by gold. For measurement of electron mobility, given the values of the LUMO energies, Ca injecting electrodes were selected. However, when such electrodes came into contact with the compounds, the metal was oxidized immediately. As a consequence, two other kinds of electron injecting electrodes were tried: Al and ZnO. Al did not show any electron injecting behavior, but ZnO did, despite the energy mismatch between its conduction band and the LUMO level of the studied compounds. Electron mobility measurements were then carried out in cells with two identical ZnO electrodes.

All such cells, both for electron and for hole mobility measurements, were filled by capillarity by heating the material above the isotropic liquid transition and, after sample filling, by cooling the cell to room temperature. The details of sample preparation and mobility measurement are included in the Supporting Information.

Several thermal treatments were performed in an effort to obtain long-range, uniform alignment of the columns over large areas of the samples. However, such attempts were not successful, and, as shown by optical microscopy, all measurements were performed on polydomain samples. The consequence of such nonuniform alignment is that the measured mobility was different in different positions of the same sample. In particular, for both holes and electrons, all measurements fell within two different ranges separated by 3−4 orders of magnitude: no mobility measurement gave results within the "empty" range. In addition, in the same sample area defined by the electrode, mobility had a tendency to increase with time: often, a first measurement performed immediately after sample preparation (cooling) fell in the low mobility range, while the same measurement carried out a few days or weeks later fell within the higher mobility range. This was particularly evident in the case of $T3C_4$-TPC_4, which forms a glassy phase upon cooling, followed by slow formation of the columnar mesophase. However, similar behavior was also observed with the other two compounds, albeit less frequently, and this suggests a tendency toward self-healing of defects in this class of materials. A decrease in mobility with time was not observed in any sample. In the case of $T3C_4$-TPC_{10}, mobilities in the higher mobility range were not measured.

DOI: 10.1021/jacs.6b06792
J. Am. Chem. Soc. 2016, 138, 12511−12518

The results, taken as average values from different positions and different samples, are listed in Table 3. The mobility values in the low range are typical of amorphous or highly disordered phases. The higher mobility values can be considered as arising from areas of the sample with a more uniform director orientation and/or a director orientation closer to the normal to the electrodes. As always with SCLC measurements, the values can be considered as an estimate of the lower limit for the mobility in the columnar phase.

The lack of director uniformity in the samples is reflected by the large standard deviations for the measured mobilities. In addition, different compounds showed different tendencies to form larger domains regardless of their orientation. For these reasons, it does not seem reasonable to compare the mobilities of the three studied compounds to establish a structure/property relationship.

In contrast, data should be discussed in terms of mobility for the whole class of materials. Measurements show that columnar phases formed by T3C$_4$-TPC$_n$ exhibit ambipolar charge transport, with hole mobilities in the 10^{-3}–10^{-2} cm^2 V^{-1} s^{-1} range and electron mobilities in the 10^{-2}–10^{-1} cm^2 V^{-1} s^{-1} range. Such mobility values for holes and electrons are in the medium-high range when compared to the mobilities observed in other, nonambipolar columnar phases. The same can be said when considering the mobilities measured in other ambipolar smectic phases[67] or phases obtained by using donor–acceptor dyads,[68] polymers,[69−72] or even solid solutions.[73] Particularly for triphenylene materials, hole mobility values have been reported in the range of 10^{-4}–10^{-1} cm^2 V^{-1} s^{-1}.[15,24−30] In a few cases, electron mobilities have been measured, obtaining values as fast as for hole mobility, in the range of 10^{-3}–10^{-1} cm^2 V^{-1} s^{-1} by the TOF method.[15] If we take into account ambipolar columnar structures with segregated stacks of donors and acceptors, as in our case, both the electron and the hole mobilities exhibited by T3C$_4$-TPC$_n$ are about 1–2 orders of magnitude higher than those reported in the literature for similar systems.[45,51]

CONCLUSIONS

Supramolecular hydrogen-bonded complexes between a tris(triazolyl)triazine derivative (T3C$_4$) and triphenylene-containing benzoic acids (A-TPC$_{10}$, ATPC$_6$, and A-TPC$_4$) have been prepared. Evidence for the formation of the 1:3 supramolecular complexes was obtained from studies in the mesophase by different techniques, such as infrared sprectroscopy and solid-state NMR (^{13}C CPMAS). All of the complexes, which are formed by nonmesogenic components, show hexagonal columnar mesomorphism at room temperature with intracolumnar order and segregated tris(triazoly)triazine and triphenylene cores, as deduced from X-ray diffraction studies and confirmed by electron density distribution maps. The supramolecular complexes exhibit ambipolar charge transport properties, with electron mobilities roughly 1 order of magnitude higher than hole mobilities.

This novel supramolecular/columnar approach has proven to be a versatile way to obtain ordered functional liquid crystals with a coaxial nanosegregation of donors and acceptors. The highly ordered triphenylene-containing structures obtained in this work are very promising for applications as organic semiconductors.

ASSOCIATED CONTENT

Supporting Information

The Supporting Information is available free of charge on the ACS Publications website at DOI: 10.1021/jacs.6b06792.

Experimental procedures (synthesis and characterization) and characterization of the supramolecular complexes (DSC thermograms, IR spectra, cyclic voltammograms, and charge mobility measurements) (PDF)

AUTHOR INFORMATION

Corresponding Authors

*rgimenez@unizar.es

*tsierra@unizar.es

Notes

The authors declare no competing financial interest.

ACKNOWLEDGMENTS

This work was financially supported by the MINECO-FEDER funds (projects MAT2015-66208-C3-1-P, CTQ2015-70174-P, MAT2012-38538-CO3-02), the Gobierno de Aragón-FSE (E04 research group and EPIF grant to B.F.), and the Gobierno Vasco (Project IT 1130-16). A.G. acknowledges support from the ELIOTROPO project (PON03PE_00092_2). R.T. was supported by MIUR under the PRIN 2012JHFYMC project. We would like to acknowledge the use of "Servicios Científico-Técnicos" of CEQMA (UZ-CSIC).

REFERENCES

(1) Mas-Torrent, M.; Rovira, C. *Chem. Rev.* **2011**, *111*, 4833–4856.
(2) Aida, T.; Meijer, E. W.; Stupp, S. I. *Science* **2012**, *335*, 813–817.
(3) Moulin, E.; Cid, J.-J.; Giuseppone, N. *Adv. Mater.* **2013**, *25*, 477–487.
(4) Jain, A.; George, S. J. *Mater. Today* **2015**, *18*, 206–214.
(5) Pisula, W.; Zorn, M.; Chang, J. Y.; Müllen, K.; Zentel, R. *Macromol. Rapid Commun.* **2009**, *30*, 1179–1202.
(6) O'Neill, M.; Kelly, S. M. *Adv. Mater.* **2011**, *23*, 566–584.
(7) Fleischmann, E.-K.; Zentel, R. *Angew. Chem., Int. Ed.* **2013**, *52*, 8810–8827.
(8) Funahashi, M. *J. Mater. Chem. C* **2014**, *2*, 7451–7459.
(9) Laschat, S.; Baro, A.; Steinke, N.; Giesselmann, F.; Haegele, C.; Scalia, G.; Judele, R.; Kapatsina, E.; Sauer, S.; Schreivogel, A.; Tosoni, M. *Angew. Chem., Int. Ed.* **2007**, *46*, 4832–4887.
(10) Kumar, S. *Chemistry of Discotic Liquid Crystals: From Monomers to Polymers*; CRC Press, Taylor & Francis Group: Boca Raton, FL, 2011.
(11) Woehrle, T.; Wurzbach, I.; Kirres, J.; Kostidou, A.; Kapernaum, N.; Litterscheidt, J.; Haenle, J. C.; Staffeld, P.; Baro, A.; Giesselmann, F.; Laschat, S. *Chem. Rev.* **2016**, *116*, 1139–1241.
(12) Sergeyev, S.; Pisula, W.; Geerts, Y. H. *Chem. Soc. Rev.* **2007**, *36*, 1902–1929.
(13) Kaafarani, B. R. *Chem. Mater.* **2011**, *23*, 378–396.
(14) Mathews, M.; Achalkumar, A. S.; Li, Q. In *Anisotropic Nanomaterials: Preparation, Properties, and Applications*; Li, Q., Ed.; Springer International Publishing: Cham, 2015; pp 241–287.
(15) Iino, H.; Hanna, J. *Opto-Electron. Rev.* **2005**, *13*, 295–302.
(16) Zaumseil, J.; Sirringhaus, H. *Chem. Rev.* **2007**, *107*, 1296–1323.
(17) Iino, H.; Hanna, J.; Bushby, R. J.; Movaghar, B.; Whitaker, B. J.; Cook, M. J. *Appl. Phys. Lett.* **2005**, *87*, 132102.
(18) Iino, H.; Takayashiki, Y.; Hanna, J.; Bushby, R. J. *Jpn. J. Appl. Phys., Part 2* **2005**, *44*, L1310–L1312.
(19) Monobe, H.; Shimizu, Y.; Okamoto, S.; Enomoto, H. *Mol. Cryst. Liq. Cryst.* **2007**, *476*, 277–287.
(20) Chen, L.-Y.; Chien, F.-H.; Liu, Y.-W.; Zheng, W.; Chiang, C.-Y.; Hwang, C.-Y.; Ong, C.-W.; Lan, Y.-K.; Yang, H. C. *Org. Electron.* **2013**, *14*, 2065–2070.
(21) Liu, X.; Usui, T.; Hanna, J. *Chem. Mater.* **2014**, *26*, 5437–5440.
(22) Kushida, T.; Shuto, A.; Yoshio, M.; Kato, T.; Yamaguchi, S. *Angew. Chem., Int. Ed.* **2015**, *54*, 6922–6925.
(23) Pal, S. K.; Setia, S.; Avinash, B. S.; Kumar, S. *Liq. Cryst.* **2013**, *40*, 1769–1816.

DOI: 10.1021/jacs.6b06792
J. Am. Chem. Soc. 2016, 138, 12511–12518

(24) Adam, D.; Closs, F.; Frey, T.; Funhoff, D.; Haarer, D.; Ringsdorf, H.; Schuhmacher, P.; Siemensmeyer, K. *Phys. Rev. Lett.* **1993**, *70*, 457−460.
(25) Adam, D.; Schuhmacher, P.; Simmerer, J.; Haussling, L.; Siemensmeyer, K.; Etzbach, K. H.; Ringsdorf, H.; Haarer, D. *Nature* **1994**, *371*, 141−143.
(26) vandeCraats, A. M.; Warman, J. M.; deHaas, M. P.; Adam, D.; Simmerer, J.; Haarer, D.; Schuhmacher, P. *Adv. Mater.* **1996**, *8*, 823−826.
(27) Paraschiv, I.; Giesbers, M.; van Lagen, B.; Grozema, F. C.; Abellon, R. D.; Siebbeles, L. D. A.; Marcelis, A. T. M.; Zuilhof, H.; Sudholter, E. J. R. *Chem. Mater.* **2006**, *18*, 968−974.
(28) Paraschiv, I.; de Lange, K.; Giesbers, M.; van Lagen, B.; Grozema, F. C.; Abellon, R. D.; Siebbeles, L. D. A.; Sudholter, E. J. R.; Zuilhof, H.; Marcelis, A. T. M. *J. Mater. Chem.* **2008**, *18*, 5475−5481.
(29) Hirai, Y.; Monobe, H.; Mizoshita, N.; Moriyama, M.; Hanabusa, K.; Shimizu, Y.; Kato, T. *Adv. Funct. Mater.* **2008**, *18*, 1668−1675.
(30) Osawa, T.; Kajitani, T.; Hashizume, D.; Ohsumi, H.; Sasaki, S.; Takata, M.; Koizumi, Y.; Saeki, A.; Seki, S.; Fukushima, T.; Aida, T. *Angew. Chem., Int. Ed.* **2012**, *51*, 7990−7993.
(31) Struijk, C. W.; Sieval, A. B.; Dakhorst, J. E. J.; van Dijk, M.; Kimkes, P.; Koehorst, R. B. M.; Donker, H.; Schaafsma, T. J.; Picken, S. J.; van de Craats, A. M.; Warman, J. M.; Zuilhof, H.; Sudholter, E. J. R. *J. Am. Chem. Soc.* **2000**, *122*, 11057−11066.
(32) An, Z. S.; Yu, J. S.; Jones, S. C.; Barlow, S.; Yoo, S.; Domercq, B.; Prins, P.; Siebbeles, L. D. A.; Kippelen, B.; Marder, S. R. *Adv. Mater.* **2005**, *17*, 2580−2583.
(33) Funahashi, M.; Sonoda, A. *J. Mater. Chem.* **2012**, *22*, 25190−25197.
(34) Gearba, R. I.; Lehmann, M.; Levin, J.; Ivanov, D. A.; Koch, M. H. J.; Barberá, J.; Debije, M. G.; Piris, J.; Geerts, Y. H. *Adv. Mater.* **2003**, *15*, 1614−1618.
(35) Lehmann, M.; Kestemont, G.; Aspe, R. G.; Buess-Herman, C.; Koch, M. H. J.; Debije, M. G.; Piris, J.; de Haas, M. P.; Warman, J. M.; Watson, M. D.; Lemaur, V.; Cornil, J.; Geerts, Y. H.; Gearba, R.; Ivanov, D. A. *Chem. - Eur. J.* **2005**, *11*, 3349−3362.
(36) Liu, X.-Y.; Usui, T.; Hanna, J. *Chem. - Eur. J.* **2014**, *20*, 14207−14212.
(37) Yamamoto, Y.; Fukushima, T.; Suna, Y.; Ishii, N.; Saeki, A.; Seki, S.; Tagawa, S.; Taniguchi, M.; Kawai, T.; Aida, T. *Science* **2006**, *314*, 1761−1764.
(38) Charvet, R.; Yamamoto, Y.; Sasaki, T.; Kim, J.; Kato, K.; Takata, M.; Saeki, A.; Seki, S.; Aida, T. *J. Am. Chem. Soc.* **2012**, *134*, 2524−2527.
(39) Jonkheijm, P.; Stutzmann, N.; Chen, Z.; de Leeuw, D. M.; Meijer, E. W.; Schenning, A. P. H. J.; Wuerthner, F. *J. Am. Chem. Soc.* **2006**, *128*, 9535−9540.
(40) López-Andarias, J.; Rodríguez, M. J.; Atienza, C.; López, J. L.; Mikie, T.; Casado, S.; Seki, S.; Carrascosa, J. L.; Martín, N. *J. Am. Chem. Soc.* **2015**, *137*, 893−897.
(41) Mahlstedt, S.; Janietz, D.; Stracke, A.; Wendorff, J. H. *Chem. Commun.* **2000**, 15−16.
(42) Tchebotareva, N.; Yin, X. M.; Watson, M. D.; Samori, P.; Rabe, J. P.; Müllen, K. *J. Am. Chem. Soc.* **2003**, *125*, 9734−9739.
(43) Samori, P.; Yin, X. M.; Tchebotareva, N.; Wang, Z. H.; Pakula, T.; Jackel, F.; Watson, M. D.; Venturini, A.; Müllen, K.; Rabe, J. P. *J. Am. Chem. Soc.* **2004**, *126*, 3567−3575.
(44) Kumar, S.; Naidu, J. J.; Varshney, S. K. *Mol. Cryst. Liq. Cryst.* **2004**, *411*, 1397−1404.
(45) Mativetsky, J. M.; Kastler, M.; Savage, R. C.; Gentilini, D.; Palma, M.; Pisula, W.; Müllen, K.; Samori, P. *Adv. Funct. Mater.* **2009**, *19*, 2486−2494.
(46) Geerts, Y. H.; Debever, O.; Amato, C.; Sergeyev, S. *Beilstein J. Org. Chem.* **2009**, *5*, 49.
(47) Hayashi, H.; Nihashi, W.; Umeyama, T.; Matano, Y.; Seki, S.; Shimizu, Y.; Imahori, H. *J. Am. Chem. Soc.* **2011**, *133*, 10736−10739.
(48) Dössel, L. F.; Kamm, V.; Howard, I. A.; Laquai, F.; Pisula, W.; Feng, X.; Li, C.; Takase, M.; Kudernac, T.; De Feyter, S.; Müllen, K. *J. Am. Chem. Soc.* **2012**, *134*, 5876−5886.
(49) Gupta, S. K.; Raghunathan, V. A.; Kumar, S. *New J. Chem.* **2009**, *33*, 112−118.
(50) Kong, X.; He, Z.; Zhang, Y.; Mu, L.; Liang, C.; Chen, B.; Jing, X.; Cammidge, A. N. *Org. Lett.* **2011**, *13*, 764−767.
(51) Zhao, K.-Q.; An, L.-L.; Zhang, X.-B.; Yu, W.-H.; Hu, P.; Wang, B.-Q.; Xu, J.; Zeng, Q.-D.; Monobe, H.; Shimizu, Y.; Heinrich, B.; Donnio, B. *Chem. - Eur. J.* **2015**, *21*, 10379−10390.
(52) Eichhorn, S. H.; Fox, N.; Bornais, B. *MRS Symp. Proc.* **2005**, *836*, 89−91.
(53) Bisoyi, H. K.; Kumar, S. *Tetrahedron Lett.* **2008**, *49*, 3628−3631.
(54) Yasuda, T.; Shimizu, T.; Liu, F.; Ungar, G.; Kato, T. *J. Am. Chem. Soc.* **2011**, *133*, 13437−13444.
(55) Umesh, C. P.; Gangarapu, S.; Marcelis, A. T. M.; Zuilhof, H. *Liq. Cryst.* **2014**, *41*, 1862−1872.
(56) Umesh, C. P.; Marcelis, A. T. M.; Zuilhof, H. *Liq. Cryst.* **2015**, *42*, 1269−1279.
(57) Umesh, C. P.; Marcelis, A. T. M.; Zuilhof, H. *Liq. Cryst.* **2015**, *42*, 1450−1459.
(58) Lehmann, M.; Huegel, M. *Angew. Chem., Int. Ed.* **2015**, *54*, 4110−4114.
(59) Zhao, K.-Q.; Bai, X.-Y.; Xiao, B.; Gao, Y.; Hu, P.; Wang, B.-Q.; Zeng, Q.-D.; Wang, C.; Heinrich, B.; Donnio, B. *J. Mater. Chem. C* **2015**, *3*, 11735−11746.
(60) (a) Hu, N.; Shao, R.; Shen, Y.; Chen, D.; Clark, N. A.; Walba, D. M. *Adv. Mater.* **2014**, *26*, 2066−2071. (b) Bag, S.; Maingi, V.; Maiti, P. K.; Yelk, J.; Glaser, M. A.; Walba, D. M.; Clark, N. A. *J. Chem. Phys.* **2015**, *143*, 144505.
(61) Percec, V.; Glodde, M.; Bera, T. K.; Miura, Y.; Shiyanovskaya, I.; Singer, K. D.; Balagurusamy, V. S. K.; Heiney, P. A.; Schnell, I.; Rapp, A.; Spiess, H. W.; Hudson, S. D.; Duan, H. *Nature* **2002**, *417*, 384−387.
(62) Beltrán, E.; Serrano, J. L.; Sierra, T.; Giménez, R. *Org. Lett.* **2010**, *12*, 1404−1407.
(63) Beltrán, E.; Serrano, J. L.; Sierra, T.; Giménez, R. *J. Mater. Chem.* **2012**, *22*, 7797−7805.
(64) Beltrán, E.; Garzoni, M.; Feringán, B.; Vancheri, A.; Barberá, J.; Serrano, J. L.; Pavan, G. M.; Giménez, R.; Sierra, T. *Chem. Commun.* **2015**, *51*, 1811−1814.
(65) Feringán, B.; Romero, P.; Serrano, J. L.; Giménez, R.; Sierra, T. *Chem. - Eur. J.* **2015**, *21*, 8859−8866.
(66) Folcia, C. L.; Alonso, I.; Ortega, J.; Etxebarria, J.; Pintre, I.; Ros, M. B. *Chem. Mater.* **2006**, *18*, 4617−4626.
(67) Funahashi, M.; Zhang, F.; Tamaoki, N. *Adv. Mater.* **2007**, *19*, 353−358.
(68) Hizume, Y.; Tashiro, K.; Charvet, R.; Yamamoto, Y.; Saeki, A.; Seki, S.; Aida, T. *J. Am. Chem. Soc.* **2010**, *132*, 6628−6629.
(69) Kim, I.-B.; Khim, D.; Jang, S.-Y.; Kim, J.; Yu, B.-K.; Kim, Y.-A.; Kim, D.-Y. *Org. Electron.* **2015**, *26*, 251−259.
(70) Li, P.; Xu, L.; Shen, H.; Duan, X.; Zhang, J.; Wei, Z.; Yi, Z.; Di, C.-a.; Wang, S. *ACS Appl. Mater. Interfaces* **2016**, *8*, 8620−8626.
(71) Nakano, K.; Nakano, M.; Xiao, B.; Zhou, E.; Suzuki, K.; Osaka, I.; Takimiya, K.; Tajima, K. *Macromolecules* **2016**, *49*, 1752−1760.
(72) Stalder, R.; Puniredd, S. R.; Hansen, M. R.; Koldemir, U.; Grand, C.; Zajaczkowski, W.; Müllen, K.; Pisula, W.; Reynolds, J. R. *Chem. Mater.* **2016**, *28*, 1286−1297.
(73) Xu, X.; Xiao, T.; Gu, X.; Yang, X.; Kershaw, S. V.; Zhao, N.; Xu, J.; Miao, Q. *ACS Appl. Mater. Interfaces* **2015**, *7*, 28019−28026.

DOI: 10.1021/jacs.6b06792
J. Am. Chem. Soc. 2016, 138, 12511−12518